A Fingerprint Verification System Based on Triangular Matching and Dynamic Time Warping

Zsolt Miklós Kovács-Vajna, *Senior Member*, *IEEE*

Abstract—An effective fingerprint verification system is presented. It assumes that an existing reference fingerprint image must validate the identity of a person by means of a test fingerprint image acquired online and in real-time using *minutiae* matching. The matching system consists of two main blocks: The first allows for the extraction of essential information from the reference image offline, the second performs the matching itself online. The information is obtained from the reference image by filtering and careful *minutiae* extraction procedures. The fingerprint identification is based on triangular matching to cope with the strong deformation of fingerprint images due to static friction or finger rolling. The matching is finally validated by Dynamic Time Warping. Results reported on the NIST Special Database 4 reference set, featuring 85 percent correct verification (15 percent false negative) and 0.05 percent false positive, demonstrate the effectiveness of the verification technique.

Index Terms—Fingerprint, fingerprint verification, dynamic time warping, triangular matching, NIST sdb 4.

1 Introduction

Fingerprints are produced by graphical flow-like ridges and valleys on human fingers. Due to their uniqueness and immutability, fingerprints are today the most widely used biometric features. Using current technology, fingerprint identification is in fact much more reliable than other possible personal identification methods based on signature, face, or speech alone [1]. Systems based on mixed biometric features, for example, fingerprint combined with face recognition, naturally improve the reliability at a higher complexity and cost [2]. Although fingerprint verification is usually associated with criminal identification and police work [3], it has become more popular in civilian applications, such as access control, financial security and verification of firearm purchasers, etc. In other words, fingerprints are a sort of identity card that people carry with them continuously.

Since manual fingerprint verification is extremely tedious and time-consuming, automatic fingerprint identification systems are in great demand. The main points addressed in automatic systems are: fingerprint acquisition, verification, identification, and classification. The identification problem is a particular case of "point pattern matching" [4], where no border correlation can be used to improve the matching efficiency since the detected minutiae belong intrinsically to a bidimensional domain without defined edges.

Fingerprint acquisition is used to obtain the fingerprint image in some useful format. There are papers showing optical [5] or capacitive [6] sensor-based methodologies. The most common technique is the inked impression widely used by the police. Optical sensors are common for automatic systems but they are easy to fool if they are used alone. Due to the prism and optics, their size cannot be reduced to portable applications. Capacitive sensors are based on the difference between the dielectric constant of the air and the human skin. These sensors require touching a sort of capacitor array and since they do not need optics, they can be sufficiently small to be included in portable systems, such as cellular phones or watches.

Fingerprint identity verification requires some knowledge of the person to be identified. The system is asked to accept or reject the hypothesis of matching between a stored fingerprint image and the test image. Consequently, the system must match the person's characteristics directly against those stored as reference information. Identity recognition requires further efforts. The system must match the characteristic of the person to be recognized against the whole set of characteristics stored in the database, thus deciding if one of the items of reference information is sufficiently similar to the one considered. Due to the huge number of images to be sought, particular techniques are used to create geometric keys for hashing tables [7] based on rotation invariant properties of triangles having minutiae as vertices. The system presented in this paper verifies the identity, rather than recognizing the person and is based on *minutiae* matching. Since different countries require a different number of *minutiae* as court evidence, the choice of *minutiae* matching instead of a more general structure matching allows for an easy customization according to the local law when required.

The paper is organized as follows: Section 2 outlines the overall system architecture and details its components in the corresponding subsections; results follow on the NIST special database 4 [8], a standard reference fingerprint

- *The author is with the Dipartimento di Elettronica per l' Automazione—DEA, University of Brescia, Via Branze 38, 25123 Brescia, Italy. E-mail: zkovacs@ing.unibs.it.*

Manuscript received 08 July 1999; revised 15 June 2000; accepted 22 Aug. 2000.
Recommended for acceptance by I. Dinstein.
For information on obtaining reprints of this article, please send e-mail to: tpami@computer.org, and reference IEEECS Log Number 110203.

0162-8828/00/$10.00 © 2000 IEEE

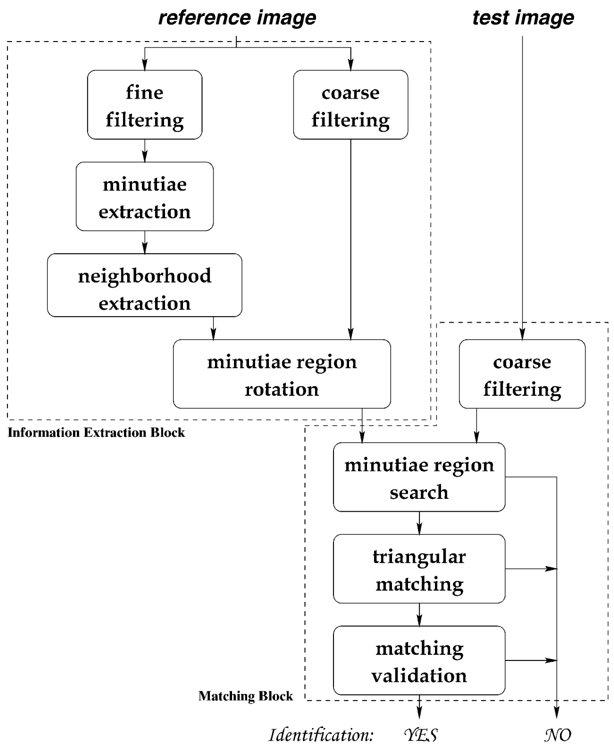

Fig. 1. Flow-chart of the identification system.

database containing severely deformed and difficult images. Some conclusions end the paper.

2 The System

Fig. 1 shows the block-diagram of the fingerprint matching system. The system compares two fingerprint images: a reference image and a test image. It is assumed that a reference image is available for the person to be identified and that it may be processed offline. The test image is obtained and used in real-time. It has to be compared to the reference image within a short time compatible with the application.

The operation sequence applied to the reference image is shown in the "Information Extraction Block" and the effective fingerprint matching is carried out on each test image, as shown in the "Matching Block." The reference image is carefully filtered to reduce noise and to use the whole gray-scale dynamics. Since this operation is performed only once for each person to be identified, the filtering operation speed is not a primary requirement. *Minutiae* detection follows. Thanks to the high-quality image, the false *minutiae* at this point are less than 10 percent of the extracted minutiae [9]. The *minutiae* coordinates and the neighboring *minutiae* list is extracted for each detected *minutiae*. A coarse and fast filter is applied to the original reference image and the region of 16×16 pixels around each *minutiae* point is saved in several rotated versions to cope with a possible significant global rotation.

The test image is acquired by the same device as the reference image. It is filtered by the same coarse filter applied to the reference image leading to comparable images. The filtered test image is scanned by a moving window technique [10] searching for possible correspondences between the reference *minutiae* regions and the test image. If some correspondences are found, a triangular matching is applied and a possible fingerprint matching is defined. Finally, this tentative matching has to be verified by Dynamic Time Warping [11] to overcome the strong local deformations. This latter verification step corresponds to the ridge count required by a legal fingerprint verification [3].

2.1 Information Extraction Block

The procedures of this block are applied to the reference image only. The main result of this processing is the real *minutiae* set of the fingerprint, minimizing the false *minutiae* and maximizing the true ones.

2.1.1 Fine and Coarse Filtering

Two different filters are applied to the reference image: a fine and a coarse one. The test image will be only coarsely filtered due to the time constraints.

The fine filter should reduce the noise as much as possible to facilitate the subsequent *minutiae* extraction operations. The specific filter used in this work is the one employed in the PCASYS package [12] built by researchers at NIST. The filter is based on the bidimensional Fourier transform and some nonlinear operators in the frequency domain in order to reduce low and high frequency noise. This specific filter was successfully applied both to paper-scanned images [8] and to those acquired by a capacitive sensor [6]. In Fig. 2, a paper-scanned image is shown on the left and the corresponding fine-filtered image is shown in the center.

The image quality is improved by the coarse filtering procedure, expanding the gray-scale dynamics to the whole pixel depth. There are several reasons why the fingerprint image does not cover the whole gray-scale dynamics: insufficient contrast or illumination, uneven ink distribution on the paper, shallow valleys, dirty fingertips, humidity, etc. When different gray-scale images are compared, some with strong contrast and some without, it is very useful to equalize the signal amplitude, which in this case is the gray value. The coarse filter does not cope with the noise in the frequency domain nor with ridge or valley interruptions. Since this filter is applied both on the reference and test images, it has to be fast and therefore simple. The coarse filtering procedure consists of the subsequent steps:

1. A four-neighbor average filter is applied to each pixel in the image to blur the image, reducing sharp local variations.
2. The image is split into $m \times n$ regions, creating approximately 16×16 pixel squares.
3. The average, maximum, and minimum pixel values are computed for each region.
4. A four-neighbor average filter is used to equalize the average, maximum, and minimum pixel values of the whole image.
5. The new pixel value is computed for each point in the image according to the formula:

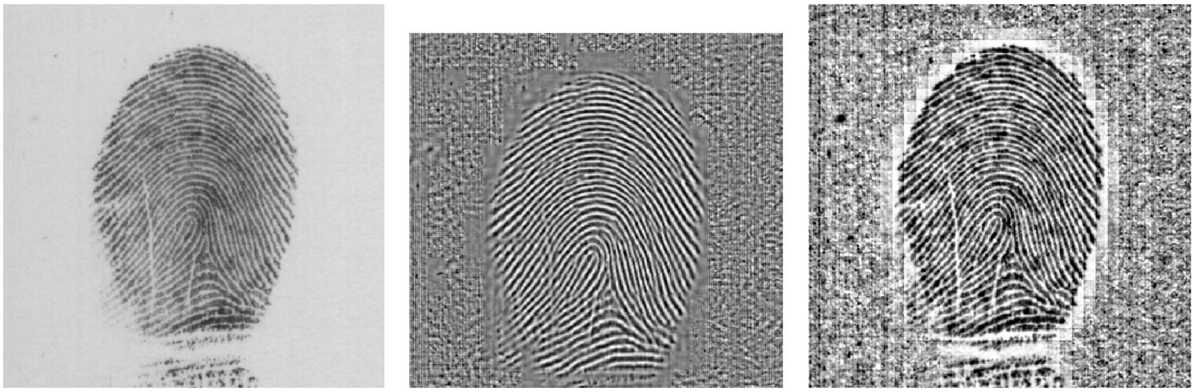

Fig. 2. Original paper-scanned image on the left, the corresponding finely-filtered image in the center, and coarsely-filtered image on the right.

$$p_n = \begin{cases} p > avg: & \dfrac{p - avg}{max - avg} \times hmx + hmx \\ p \leq avg: & \dfrac{avg - p}{avg - min} \times hmx, \end{cases}$$

where p_n is the new pixel value, p is the old pixel value, avg, max, and min are the average, maximum, and minimum pixel values in the region, and hmx is half of the maximum possible pixel value ($hmx = 128$ for 8 bit pixels).

The rightmost image of Fig. 2 shows the filtered image. In the filtered image, better contrast is evident but also the above defined regions are clearly visible. However, these blocks and the background noise have no adverse effect because the reference image has already been finely filtered.

2.1.2 Minutiae Extraction

The *minutiae* considered in the identification systems are ridge bifurcations and terminations. The aim of this procedure is to extract the real 40-60 *minutiae* of a fingerprint image from the 500-800 contained in typical *well-filtered*, skeletonized, and binarized images of NIST sdb 4. Besides classical methodologies for removing close *minutiae*, new approaches are used for deleting spurious *minutiae* by ridge repair, short ridge elimination, and island filtering. In particular, a novel algorithm based on ridge positions is employed for bridge filtering instead of classical methods based on directional maps. Finally, two novel criteria validate the endpoints and bifurcations. The details of this methodology are in [9].

2.1.3 Neighborhood Extraction

In order to obtain correct and efficient identification, a list of *minutiae* neighbors is extracted for each *minutiae*. The *minutiae* are ordered according to the increasing distance from the image center and each list is ordered according to the increasing distance from the corresponding *minutiae*. The image center is assumed to be the mass-center of the detected *minutiae*. The *minutiae* list provides information on the *minutiae* position and on the ridge/valley behavior between *minutiae*. For this reason, the line connecting each *minutiae* and one of its neighbors is traced, and the gray values extracted. In Fig. 3, a coarsely-filtered fingerprint image is reported on the left, showing the traced lines starting from a *minutiae* in the central area. On the right, the gray-scale behavior of two lines is reported: The upper curve shows the shortest line, while the lower curve reports the gray values along the longest line. The number of lines to be traced for each *minutiae* was defined experimentally to be about 20 and they are extracted to make the line distribution as uniform as possible over the 360 degrees, depending on the detected *minutiae*.

2.1.4 Minutiae Region Rotation

Identification of *minutiae* in the test image is based on a comparison between regions surrounding the *minutiae* in the reference image and each point in the test image. A 16×16 square area is extracted around a *minutiae* in the reference image and it is matched against an area in the test image having the same shape and size. It has to take into account three effects, even if the test image represents the same fingerprint as the reference image: it may have different contrast, it may be distorted, and it may be rotated. The problem of different contrast is solved by the already defined coarse-filtering procedure. Image distortion is taken into account by defining a suitable threshold while computing the similarity of regions using the L_1 vector norm. The relative rotation of the images has to be investigated more closely in order to evaluate its effect in the similarity computation.

One hundred *minutiae* regions were extracted randomly from different images and matched against several rotated versions of the same images, computing the difference between corresponding image pairs according to the method detailed in Section 2.2.1. The graph of Fig. 4

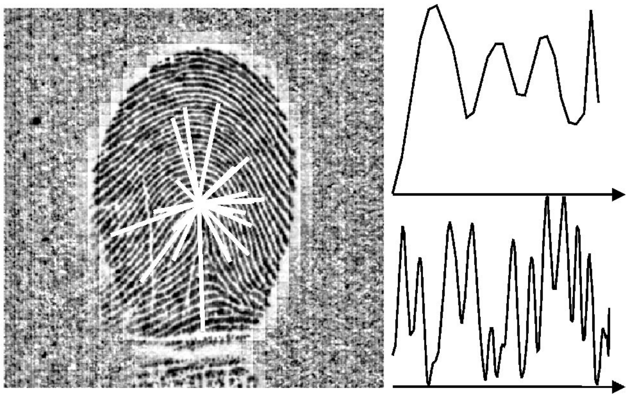

Fig. 3. *Minutiae* connecting lines traced on the fingerprint image on the left and gray value behavior on the shortest (upper) and longest (lower) lines on the right graphs.

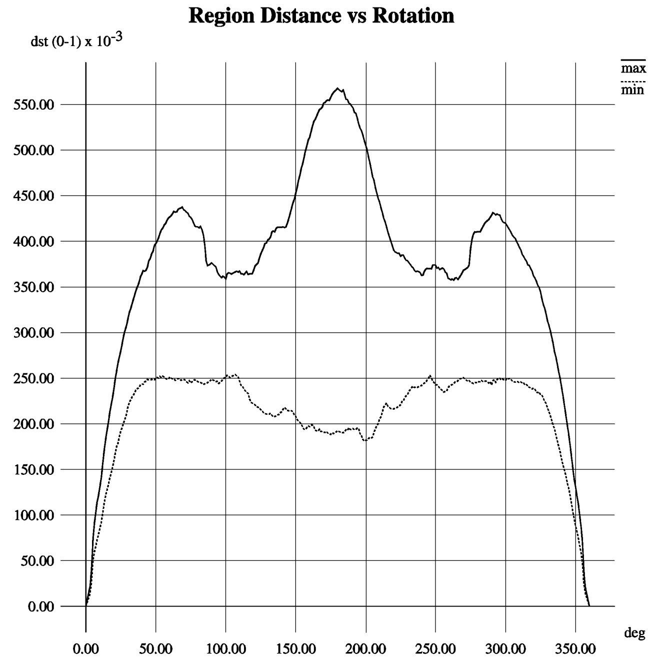

Fig. 4. Maximum (continuous line) and minimum (dotted line) normalized differences between a hundred identical region pairs as a function of the rotation angle of the second image.

shows the maximum difference (continuous line) and the minimum difference (dotted line) as a function of rotation expressed in degrees. The values are normalized by dividing the computed difference by the maximum possible difference between two images, a white and a black image, i.e., by $16 \times 16 \times 255 = 65,280$. As one may expect, the difference is zero for 0 and 360 degrees, while it is maximum for 180 degrees. This latter behavior is due to the smallest overlap of corresponding ridges and valleys in bifurcations and terminations. The manifest tri-modal behavior of the curves depends on the size of the region: In this case, up to three ridges may be included in the matched regions. Zooming the 0-10 degree area comes up that below 2.5 degrees, the normalized difference is below 2 percent. If, for example, the images may be rotated by up to 20 degrees, from Fig. 4, it is clear that rotation on its own leads to a 25 percent difference. This is comparable with the difference between two regions which do not contain the same *minutiae*, so rotation may hide the distinction between different regions. This problem can easily be solved, simply by rotating the regions surrounding the reference *minutiae* points and attempting to match each of these rotated regions instead of just the original one. By rotating each region by -15, -10, -5, 0, 5, 10, 15 degrees, the difference between two regions due to the rotation is kept below 2.5 percent up to 17.5 degrees and it may increase up to 7 percent only for a 20 degree rotation.

2.2 Matching Block

The operations of this block form the real identification procedure. The test image is compared to the reference image using the information already extracted by the "Information Extraction Block." The test image is filtered by the already described coarse filter and the *minutiae* regions of the reference image are moved around the test image searching for possible correspondence. The possible correspondences are used to obtain a match-graph which is validated by Dynamic Time Warping applied to the *minutiae* connecting lines.

2.2.1 Minutiae Region Search

The point to address is where the *minutiae* corresponding to the reference *minutiae* are found in the test image. Each *minutiae* in the reference image associates a set of rotated regions around the *minutiae* itself. The test image is scanned point by point [10] and the similarity between each rotated version of the area surrounding the reference *minutiae* and the region around the current test image point is computed.

The best similarity between each rotated version is considered and if the similarity is above a certain threshold, the current pixel is a possible candidate in the test image. For each reference *minutiae*, a small cluster of neighboring pixels results on the test image for each candidate region. The mass center of the cluster is the candidate *minutiae* point. The points are sorted in order of decreasing similarity and the first N_c ($N_c = 12$ was found experimentally in the current system) are accepted and form the basis for the subsequent matching operations. This thresholding operation and the ranking are very important because it is impossible to define a universal threshold, i.e., for a very large number of images. If the threshold is too low, in several images, too many points will become possible candidates, whereas if it is too high, some corresponding images will never associate with feature points. The ranking ensures that the correspondence will be possible in nearly all images and the number of correspondences will be controlled.

In Fig. 5, the reference image is shown as Fig. 5a. A small square is drawn around the current *minutiae* to be matched. Fig. 5c is a zoom on this region where a bifurcation point may be observed. A corresponding region should be sought in the test image. This searching procedure is based on the similarity computation between two gray-scale regions of the same size. In particular, the region around each pixel of the test image is compared to the *minutiae* region of the reference image and a possible correspondence is accepted according to the similarity of the subimages. Each region is assumed to be 16×16 pixels. Let (X_{iT}, Y_{iT}) and (X_{jR}, Y_{jR}) be the *i*th point of the test image and the *j*th point of the reference image, respectively. Let S_{iT} and S_{jR} be two surfaces associated with (X_{iT}, Y_{iT}) and (X_{jR}, Y_{jR}), respectively. A possible distance between the two regions may be defined according to the discrete integral norm:

$$N_d = \sum_x \sum_y d[S_{jR}(x - X_{iT} + X_{jR}, y - Y_{iT} + Y_{jR}), S_{iT}(x, y)]$$
$$X_{iT} - 8 \le x < X_{iT} + 8, \quad Y_{iT} - 8 \le y < Y_{iT} + 8,$$

where $d()$ is a nonnegative function. A possible choice is $d() = abs()$ leading to the L_1 norm. The value N_d is the distance between two regions around the *i*th point of the test image and the *j*th point of the reference image, respectively. Fig. 5d is the similarity map of the test image, where white points are associated with regions of insufficient similarity and dark areas indicate a possible

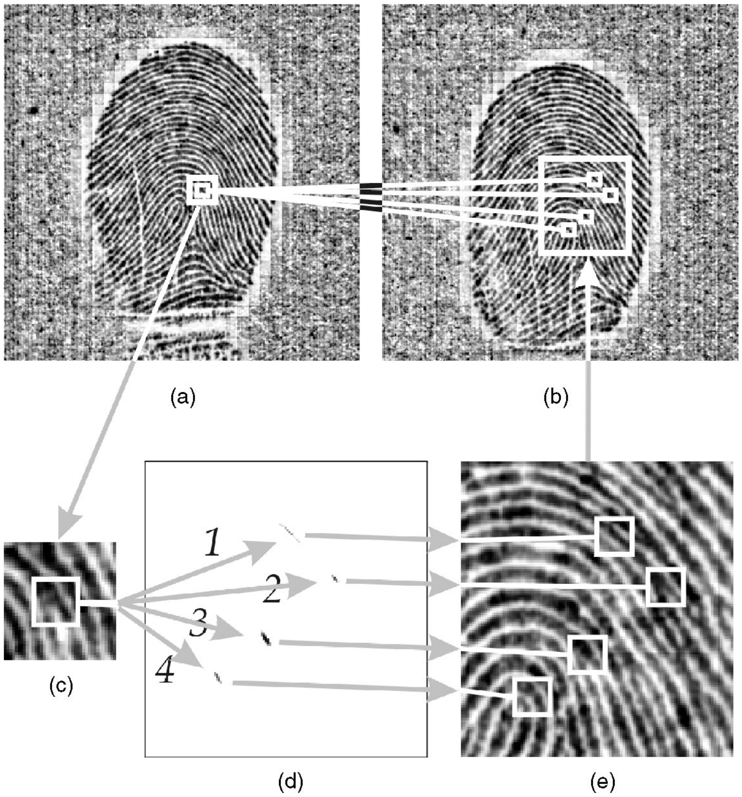

Fig. 5. (a) Reference image with *minutiae* to search for, (b) test image candidate regions, (c) zoom on the reference *minutiae*, (d) similiarity map drawn on test image, and (e) zoom on test image with the corresponding regions.

correspondence. The darker the region, the better the correspondence (meaning a smaller N_d value). In this case, four candidate regions are present. Fig. 5e shows the four candidate regions superimposed on the test image and Fig. 5b shows the overall test image. The real correspondence is between the reference *minutiae* and region 3 of the test image. Region 2 is still a bifurcation, but by looking at the *minutiae* area only, it is impossible to distinguish it from the reference *minutiae*. Regions 1 and 4 are only similar according to the metrics defining the correspondence, but there is no real feature point. Since no *minutiae* extraction is performed on the test image and only similarity computation is done with regions of the reference image, the selection of the effective matching is postponed to the subsequent identification phase. There is no point in increasing the threshold for accepting only more similar regions because on noisy images with shallow ridges or with noise of some kind, it would be impossible to define the real mapping.

2.2.2 Triangular Matching

In order to define an effective matching technique, a deformation model must be identified. When looking at different images containing the same fingerprint, a strong global deformation of the images can be observed. This distortion is due to static friction on a sensor surface, or paper, or rolling of the finger during ink-based registration techniques. However, small portions of the images do not appear to exhibit manifest distortion. The idea of how to take into account small local variations, which may lead to huge global distortion, is discussed as follows.

A pair of triangles forming a square are reported in Fig. 6, in particular in Fig. 6a. By shortening or extending some of the edges by less than 10 percent of their original length, the two images shown in Fig. 6b or Fig. 6c may be obtained. This small distortion makes the original form easily recognizable and may be comparable with the local distortion of a fingerprint image. In particular, the area around a *minutiae* may be slightly distorted due to static friction caused by the fingertip touching a hard surface. By replicating the square of Fig. 6 several times, it is possible to create a big image. A complete fingerprint image may be considered to consist of several small pieces, some of them representing *minutiae*. Fig. 7 on the left shows a cross formed from the squares of Fig. 6. On the right, the same cross is shown where the edges of the squares were shortened or extended by less than 10 percent of the original length. Such a small local distortion produces, for example, a 6 percent shortening of edge **AB** and a

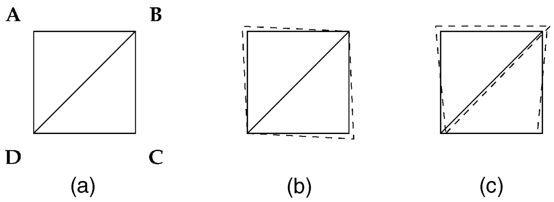

Fig. 6. (a) Two triangles forming a square, (b) and (c) distortion of the triangles, where each edge is shortened or extended by less than 10 percent of its original length.

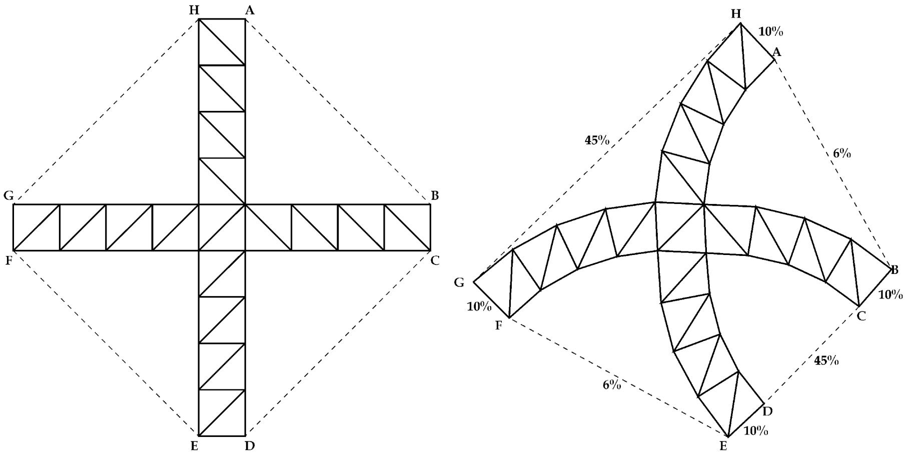

Fig. 7. Original image on the left, distorted image on the right with local deformation less than 10 percent, but consequent global deformation reaching 45 percent.

45 percent extension of edge **GH**. This simple (and exaggerated) example shows the idea of the model, which defines the distortion of fingerprint images where a small local distortion is amplified on a global basis.

The following algorithm (written in a pseudo C code) is used to extract a possible *minutiae* set where the matching is established. The result is a number of matching *minutiae* pairs on the reference and test images, which according to the required number of pairs, forms the basis of the identification. By generating a map of already considered *minutiae*, it is possible to significantly reduce the number of tentative matching maps and employ a very short computation time in this phase.

The following list contains the functions and procedures used in the algorithm:

- `GetNextMinutiae()` gets the next, already not considered, reference *minutiae* from the ordered set defined in Section 2.1.3.
- `GetNextTestMinutiae(ref)` gets the next, already not considered, test *minutiae* corresponding to `ref` *minutiae* from the ordered set with decreasing similarity between test and reference regions according to Section 2.2.1.
- `LineLength(ref1, ref2, test1, test2)` computes the length difference between the lines connecting two *minutiae* in the reference image and two in the test image. This procedure may include the verification phase shown in the next section to improve performance.
- `ComputeAngle(ref1, ref2, test1, test2)` computes the angle between two lines connecting *minutiae* pair `ref1, ref2` and pair `test1, test2`, respectively.
- `AddMatchedMinutiae(ref1, test1, ref2, test2)` adds the pairs of matched *minutiae* in reference image and in test image to the already matched *minutiae* list.
- `GetNextMinutiaePair(ref1, test1, ref2, test2)` gets the next *minutiae* pair belonging to an already matched line both in reference and test images.
- `GetNextCloseMinutiae(ref1, ref2)` gets the-next, already not considered reference *minutiae* from the ordered minutiae list minimizing the function `max(L2(ref1, ref3), L2(ref2, ref3))`, where `max()` is the larger between two real numbers and `L2()` is the Euclidean norm on the bidimensional Cartesian plane.
- `ComputeTestCoordinates(X, Y, ref3, ref1, test1, ref2, test2)` computes the (X,Y) coordinates corresponding to `ref3` using the linear roto-translation defined by the mapping `ref1` $->$ `test1`, `ref2` $->$ `test2` according to the formulae:

  $$X = \alpha x_3 + \beta y_3 + \gamma_x \qquad Y = -\beta x_3 + \alpha y_3 + \gamma_y,$$

  where

  $$\alpha = \frac{(X_2 - X_1)(x_2 - x_1) + (Y_2 - Y_1)(y_2 - y_1)}{(x_2 - x_1)^2 + (y_2 - y_1)^2}$$
  $$\beta = \frac{(X_2 - X_1)(y_2 - y_1) - (Y_2 - Y_1)(x_2 - x_1)}{(x_2 - x_1)^2 + (y_2 - y_1)^2}$$
  $$\gamma_x = X_1 - \alpha x_1 - \beta y_1$$
  $$\gamma_y = Y_1 - \alpha y_1 + \beta x_1$$

  with the uppercase variables referring to the test coordinate space and the lowercase coordinates to the reference coordinate space.
- `OrderTestMinutiae(ref, x, y)` orders the test *minutiae* corresponding to the reference *minutiae* `ref` according to the increasing distance from point of coordinate `(x, y)` in the test image.
- `NumberOfMatchedMinutiae()` computes the number of already matched minutiae.
- `MaxDistance` is the maximum allowable deformation between segments (for example, 10 percent or 6 pixels).
- `MaxAngle` allows to control the maximum rotation (for example, 20 degrees).
- `MinimumMatch` is the minimum number of required minutiae to match (for example, 14) for a valid identification.

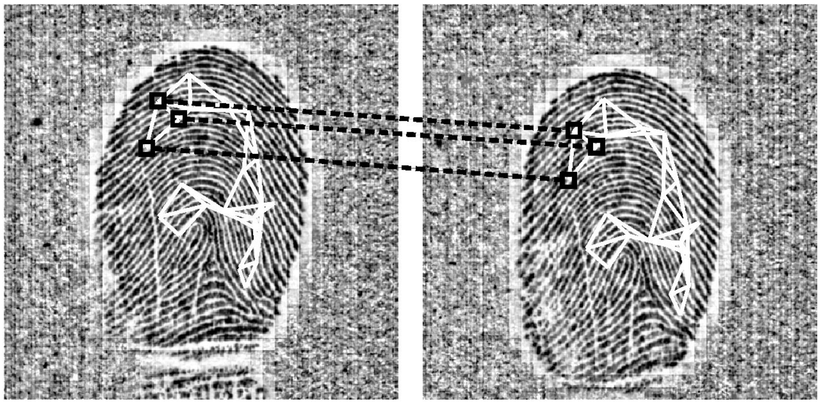

Fig. 8. Matching triangle-based graphs: reference image on the left, test image on the right.

```
/* Triangular Matching Algorithm*/:
do
  /* sets two minutiae on reference image */
  ref1 =GetNextMinutiae();
  ref2= GetNextMinutiae();
  /* sets the corresponding two minutiae
     on test image */
  do
   test1 = GetNextTestMinutiae(ref1);
   do
     test2 = GetNextTestMinutiae(ref2);
     if (test2 != null)
      dist = LineLength(ref1, ref2, test1,
            test2);
      angle = ComputeAngle(ref1, ref2, test1,
             test2);
     endif
     /* the correspondence is valid if
         deformation is
       small and rotation is allowed */
   until (dist < MaxDistance AND
         angle < MaxAngle)
      OR test2 == null
  until test2 != null OR test1 == null
  if (test1 == null OR test2 == null)
   goto end_NO_MATCH;  /* no matching can be
    defined */
  endif
  /* adds minutiae pair to already
       matched list */
  AddMatchedMinutiae(ref1, test1, ref2,
       test2);
  /* sets third minutiae for each pair
       of reference and
    test matching minutiae pairs according to
    roto-translation defined by
       the minutiae pairs */
  do
   validpair=GetNextMinutiaePair
                            (&ref1,&test1,
                             &ref2, &test2);
   if (validpair)
    do
       ref3 = GetNextCloseMinutiae(ref1, ref2);
       if (ref3 != null)
        /* defines third minutiae corresponding
            area on test image */
        ComputeTestCoordinates(&x,&y, ref3,
                              ref1,test1,
                              ref2, test2);
        OrderTestMinutiae(ref3, x, y);
       endif
       do
        test3 = GetNextTestMinutiae(ref3);
        if (test3 != null)
        dist1 = LineLength(ref1, ref3,
                         test1, test3);
        dist2 = LineLength(ref2, ref3,
                         test2, test3);
        angle1 = ComputeAngle(ref1, ref3,
                            test1, test3);
        angle2 = ComputeAngle(ref2, ref3,
                            test2, test3);
       endif
       /* the correspondence is valid
            if deformation is
         small and rotation is allowed */
      until (dist1 < MaxDistance AND
          dist2 < MaxDistance AND
          angle1 < MaxAngle AND
            angle2 < MaxAngle) OR
         test3 == null
     until test3 != null OR ref3 == null
     if (ref3 != null AND test3 != null)
      AddMatchedMinutiae(ref1, test1,
                        ref3, test3);
      AddMatchedMinutiae(ref2, test2,
                        ref3, test3);
     endif
    endif
   until validpair == false
  until NumberOfMatchedMinutiae() >
       MinimumMatch
  /* continue with validation procedure of next
  section */
```

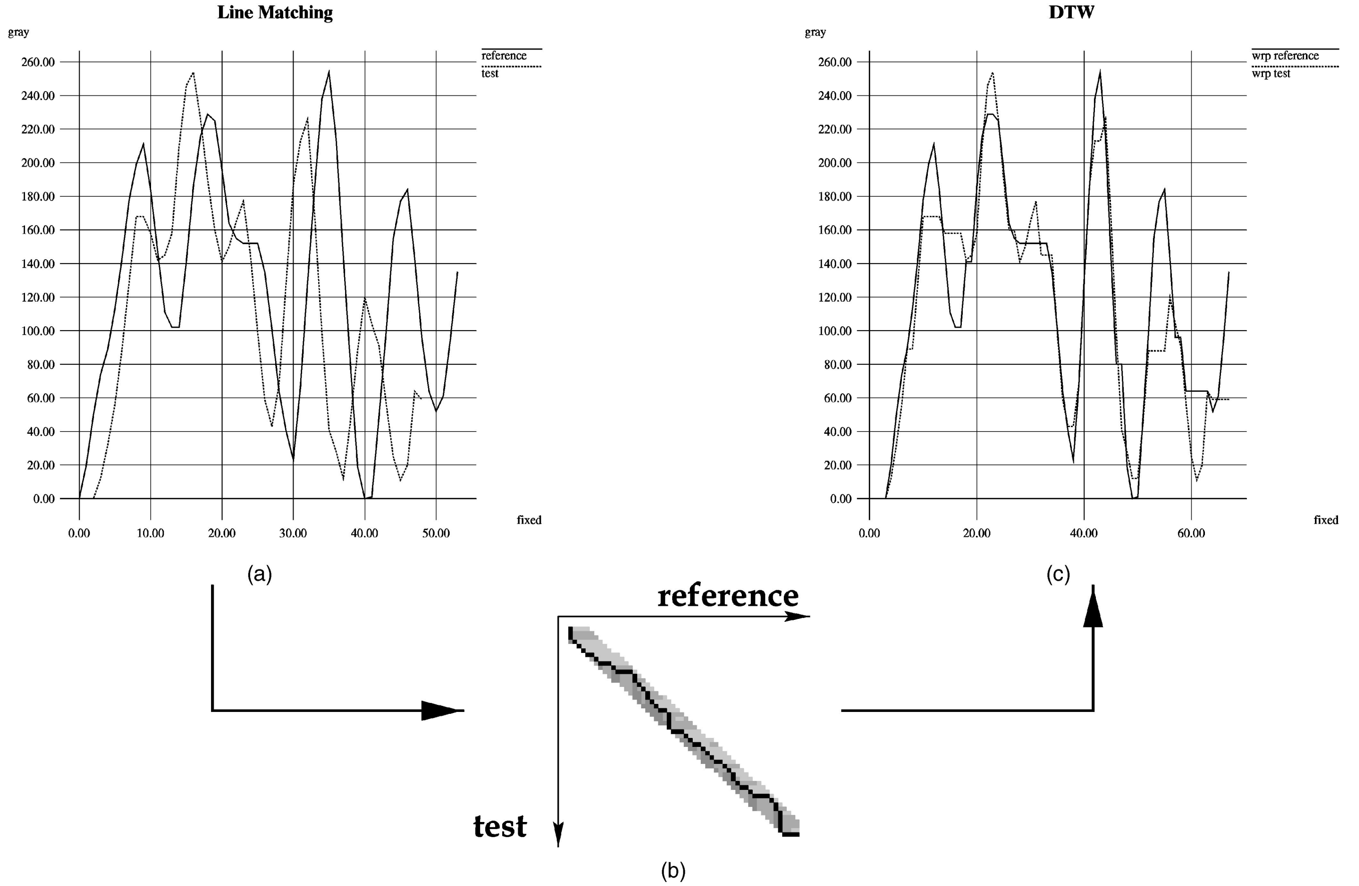

Fig. 9. Gray-scale line matching. (a) Correspinding reference and test lines, (b) deformation map, and (c) final overlapping of the two lines.

The already defined algorithm creates a connected graph on both images, where each graph is composed of triangles with shared edges. Fig. 8 shows the reference image on the left and the test image on the right in an intermediate stage of the triangular matching. The two graphs are shown in white, with the already matched *minutiae* at their vertices. Three matching *minutiae* and the connecting lines are also visible at the top of the image as dashed black lines. The upper two black squares indicate the currently extracted *minutiae* pair on the left image, and the corresponding pair on the right one. The third pair of black squares on the two images show the third coordinates, while this new *minutiae* is accepted, enlarging the already matching *minutiae* set. This procedure allows for matching on a local basis, where distortion is small, and can also identify two fingerprints with considerable global distortion.

Distortion can easily be measured using the two graphs, one on the reference image and the other on the test image, respectively, thanks to the already computed correspondence between single vertices and edges of the triangles that make up the graphs. A possible measure of the distortion is the average relative distortion of the corresponding edges of the triangles. For example, the images in Fig. 8 have a relative average distortion of 2.57 percent and a maximum distortion of 5.96 percent. Also, it is possible to define a relative translation and rotation of the images. When the images are distorted, translation and rotation are not uniquely defined. Translation may be defined as the movement of the mass-center of the two graphs relative to the image borders and rotation as the relative rotation of the graphs around the mass-center. For example, the images in Fig. 8 are translated by 1.87mm (37 pixels) and rotated by 5.44 degrees anticlockwise relative to each other.

2.2.3 Matching Validation

The science of fingerprint identification is based on both the matching of a certain number of *minutiae* and the ridge-count between *minutiae* pairs [3]. The previous matching phases are useful for matching *minutiae* between the reference and test images, but the validation procedure must be performed before effective matching can be confirmed.

In Fig. 3, some gray-scale profiles are shown on lines connecting *minutiae* pairs. The validation phase involves matching curves like those of Fig. 3 extracted from corresponding regions on the reference and test images. Since the *minutiae* matching phase does not consider global information in the images, and is based only on the local similarity of regions, gray-scale line matching yields global information and the final result of the whole identification procedure. When the images are relatively distorted, the coordinates of the *minutiae* are not defined exactly and the lines may not refer precisely to the same points in the corresponding images. The result is that a physically matching line pair do not overlap because of different

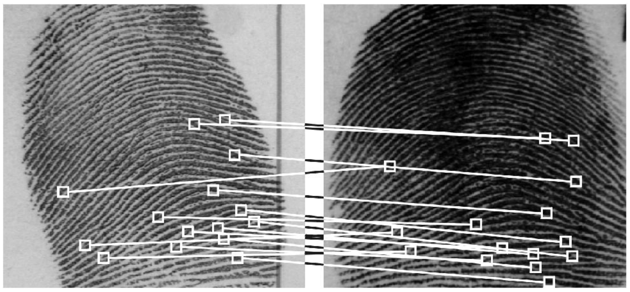

Fig. 10. Example of correctly identified fingerprints.

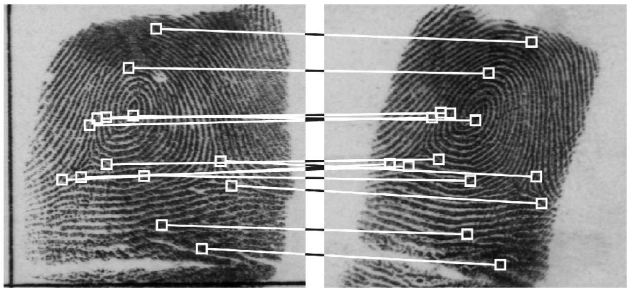

Fig. 11. Example of correctly identified fingerprints.

image contrast, deformation and different starting, or ending coordinates. The coarse-filtering technique described earlier solves the contrast problem but all the remaining problems must still be faced.

Fig. 9a shows a pair of matching lines extracted from a pair of images obtained from the same finger. The continuous line comes from the reference image, the dotted one from the test image. The two lines do not overlap for the reasons described above and a possible integral norm or some other distance computation technique alone fails in the recognition of the matching. Indeed, the same "distance" may also be observed in mismatching line pairs.

At this point, the main problem is matching of nonuniformly phase-displaced curves. The same problem is common in speech recognition, where the curves are defined in the time domain and are not uniformly delayed. This problem is overcome by Dynamic Time Warping [11], which can also be applied in fingerprint validation. Considering as time the spatial coordinate along the line connecting the two *minutiae*, the nonlinear displacement can be identified very easily. Fig. 9b shows the deformation map obtained by applying the Dynamic Time Warping technique to the curve pair of Fig. 9a with the same constraints on local deformation used during the triangular matching. The common constraints make the triangular matching and the validation phases consistent. The black curve in the allowed gray area of Fig. 9b identifies the nonlinear expansion which maximizes the overlapping of the two curves. Fig. 9c shows two curves, each of which has been distorted according to the Dynamic Time Warping result in order to minimize the difference. Application of Dynamic Time Warping to each possibly matching line pair allows for validation of the lines, i.e., validation of the *minutiae* they are connected to.

It is important to note that the *minutiae* matching and line validation methodology presented is statistically very robust. It means that since a system based on this technique must identify a certain number of validated *minutiae* in an image pair, for instance, 12 or 16 *minutiae*, even if some of the *minutiae* may not be correctly matched, the remaining *minutiae* are still able to validate the identification. This is extremely important because *minutiae*-like configurations may appear in dirty areas in low-quality images. These *minutiae* may be matched and even validated, but they are statistically insignificant.

3 Results

Results reported on any identification system should be based on a standard reference set so that they can be compared with those reported in the literature. Unfortunately, researchers working in this field report their measurements on proprietary data even though they recognize the importance of standard reference data based results [1]. There are several databases created by NIST containing fingerprint images which usually also contain very low quality images, such as NIST sdb4, 9, etc.

The fingerprint identification system was validated using the reference database "NIST Special Database 4" [8]. This database consists of 2,000 fingerprint image pairs (4,000 total). The images are obtained by scanning inked fingerprints from paper at 500dpi. The images are 8 bit/pixel and of fixed 512×512 size. The database contains good quality images and also image pairs which are severely deformed due to rolling, inking problems, dirt, or shallow ridges. About 120 image pairs out of the 2,000 (6 percent of the total) could not be matched by a human expert, a retired policeman, without image enhancement techniques, even though in these cases, classification into the five main classes was still possible. The fingerprints are mainly centered in the images, but they generally do not cover the whole image and background is nearly always present. Thanks to the *minutiae* extraction method employed in the system [9], image segmentation is not needed.

Fig. 10 shows a correctly matched fingerprint pair. In this case, 15 *minutiae* were matched. The relative image translation is 0.76mm and the average rotation is 16.9 degrees. The average image distortion is 6.72 percent, while the maximum is 15.9 percent. These parameters were calculated according to the description of Section 2.2.2.

Fig. 11 shows a correctly matched fingerprint pair with 14 matched *minutiae*. The relative image translation is 1.00mm and the average rotation is 15.8 degrees. The average image distortion is 4.62 percent, while the maximum distortion is 16.0 percent.

The identification, false negative, and false positive rates were computed using the reference database. The identification rate is the number of correctly identified image pairs divided by the total number of pairs (2,000). The false negative rate is the complement to one of the identification rates, i.e., the number of corresponding image pairs which have not been matched with sufficient accuracy divided by the total number of image pairs. The false positive rate is the number of noncorresponding image pairs which were

TABLE 1
Fingerprint Verification Results

Verif. rate	False neg. rate	False pos. rate
80%	20%	0.002%
85%	15%	0.05%

matched by the system as a percentage of the total number of checked pairs. For the false positive computation, 500,000 image pairs were selected randomly from the 4,000 fingerprints of the database.

The subsequent results were obtained by accepting a maximum relative translation of 7mm, a rotation of ±25 degrees and a maximum average deformation of 15 percent: Checking the identified image pairs, the maximum relative translation was 6.75mm, corresponding to 133 pixels, the maximum absolute rotation was 22 degrees and the maximum average distortion was 15 percent with local distortions above 50 percent.

The unmatched image pairs were checked manually. The 80 percent identification rate leads to 20 percent false negatives. On checking the 20 percent unmatched image pairs carefully, 30 percent were not recognized even by the human expert, while 70 percent were correctly identified. Of this 70 percent, 43 percent had a distortion above the permitted 15 percent threshold, 13 percent were rotated more than 25 degrees and in the remaining 44 percent, the system failed because it did not find a sufficient number of matching *minutiae*. This portion can be reduced by accepting a false positive rate: The 85 percent identification rate leads to 15 percent false negatives and to a false positive rate of 0.05 percent. On checking the 15 percent unidentified image pairs, 43 percent were again not recognized by the human expert, while 57 percent were correctly identified. Of this 57 percent, 56 percent had a distortion above the permitted 15 percent, 42 percent were rotated more than 25 degrees and in the remaining 2 percent, the system failed because it did not find a sufficient number of matching *minutiae*.

The importance of the final verification phase by dynamic time warping is evident measuring the false positive and negative rates when this block is disabled. In this case, the false negative rate remains unchanged since it is mainly due to false minutiae correspondence detection. However, the false positive increases from 0.05 percent to 10 percent at 15 percent false negative see Table 1).

The system is currently implemented in software and its performance depends on the image size and on the maximum allowed relative rotation. A closer look to the average timing of image pairs of 512 × 512 pixels on a P6@233MHz shows that the nonlinear filter based on the bidimensional Fourier transform takes about 3 seconds, while the coarse filtering needs just 0.2 seconds. The *minutiae* are detected in about 1.2 seconds. The most time consuming part of the system is the correspondence map detection defined in Section 2.2.1, which needs 7 seconds for an allowed ± 20 degree rotation. A further second is needed for the triangular matching and final verification. The correspondence map detection can be easily implemented in hardware using an already known analog-flash technology applied for *k*-nearest neighbors in optical character recognition [13], lowering the overall raw fingerprint matching time to less than 2 seconds also for 512 × 512 pixel images [14]. Using a capacitive sensor [6] of 200 × 200 pixels with a ± 5 degree rotation limit, the average overall identification time is below 1 second. There are several reasons for this speed up: the image size, its background, and the fewer *minutiae* in a smaller fingertip region.

4 Conclusions

A fingerprint verification system has been designed and implemented based on two main blocks: the information extraction block and the matching block. The first block is used to extract the information from reference images offline. The second block is used in the matching phase online. The *minutiae* correspondences are found using a triangular matching algorithm and the final verification uses Dynamic Time Warping. Triangular matching is fast and overcomes the relative nonlinear deformation present in the fingerprint image pairs. In fact, triangular matching saves local regularities and compensates for global distortion. The final verification based on Dynamic Time Warping allows a very low false positive rate to be obtained. The fingerprint matching rate and accuracy is very high, even on a difficult image database such as NIST sdb 4. Some statistics on this reference database were also reported.

Acknowledgments

The author wishes to express his appreciation to Professor R. Guerrieri and Dr. A. Ferrari for their help and encouragement on this work. The author would like to thank the NIST for providing the PCASYS package. This work was supported by ST-Microelectronics, which also owns the patent [14], and it was done at the Dipartimento di Elettronica, Informatica e Sistemistica—DEIS, University of Bologna, Viale Risorgimento 2, 40136 Bologna, Italy.

References

[1] A. Jain, L. Hong, and R. Bolle, "On-Line Fingerprint Verification," *IEEE Trans. Pattern Analysis and Machine Intelligence*, vol. 19, no. 4, Apr. 1997.

[2] L. Hong and A. Jain, "Integrating Faces and Fingerprints for Personal Identification," *IEEE Trans. Pattern Analysis and Machine Intelligence*, vol. 20, no. 12, Dec. 1998.

[3] *The Science of Fingerprints: Classification and Uses,* United States Dept. Justice, Federal Bureau of Investigation, Washington, DC, rev. 12–84, 1988.

[4] S. Umeyama, "Parameterized Point Pattern Matching and Its Application to Recognition of Object Families," *IEEE Trans. Pattern Analysis and Machine Intelligence*, vol. 15, no. 2, Feb. 1993.

[5] L. Coetzee and E. C. Botha, "Fingerprint Recognition in Low Quality Images," *Pattern Recognition*, vol. 26, no. 10, pp. 1,441–1,460, Oct. 1993.

[6] M. Tartagni and R. Guerrieri, "A 390dpi Live Fingerprint Imager Based on Feedback Capacitive Sensing Scheme," *Proc. 1997 IEEE Int'l Solid-State Circuit Conf.*, pp. 200–201, 1997.

[7] R.S. Germain, "Large Scale Systems," *Biometrics: Personal Identification in Networked Soc.*, A. Jain, R. Bolle, and S. Pankanti, eds., pp. 311–325, 1998.

[8] NIST Special Database 4, *8-Bit Gray Scale Images of Fingerprint Image Groups—(FIGS),* Image Recognition Group, Advanced Systems Division, Computer Systems Laboratory (CSL), Nat'l Inst. Standards and Technology, 1992.

[9] A. Farina, Z.M. Kovács-Vajna, and A. Leone, "Fingerprint Minutiae Extraction from Skeletonized Binary Images," *Pattern Recognition,* vol. 32, no. 5, pp. 877–889, 1999.

[10] H. Yahagi, S. Igaki, and F. Yamagishi, "Moving-Window Algorithm for Fast Fingerprint Verification," *Proc. 1990 Southeastcon,* vol. 1, pp. 343–348, 1990.

[11] L. Rabiner and B.-H. Juang, *Fundamentals of Speech Recognition,* PTR Prentice-Hall, Inc., 1993.

[12] G.T. Candela, P.J. Grother, C.I. Watson, R.A. Wilkinson, and C.L. Wilson, *PCASYS—A Pattern-Level Classification Automation System for Fingerprints,* 1995.

[13] A. Kramer, M. Sabatini, R. Canegallo, M. Chinosi, P.L. Rolandi, and P. Zabberoni, "Flash-Based Programmable Nonlinear Capacitor for Switched-Capacitor Implementation of Neural Networks," *Proc. IEEE IEDM 1994,* pp. 449–452, 1994.

[14] Z.M. Kovács-Vajna, "Fingerprint Minutiae Matching Architecture Based on Analog Flash Memory," U.S.A. Patent Application, Appl. No. 123,956, filing date: 28.07.1998 (patent pending).

Zsolt M. Kovács-Vajna (M'90-SM'00) received the Laurea degree summa cum laude and the PhD degree in electronics engineering and computer sciences from the University of Bologna, Italy, in 1988 and 1994, respectively, for his work on optical character recognition and circuit simulation techniques. He was a visiting researcher (1988-1994) and an assistant professor in Electronics (1994-1998) at the Department of Electronics Engineering, University of Bologna, Italy. Currently, he is an associate professor of Electronics at the Department of Electronics for Automation, University of Brescia, Italy, and teaches the course "Microelectronics." His research interests include integrated circuit design for sensor applications, pattern recognition (OCR, ICR, fingerprint identification, innovative pointer devices), and electromagnetic interference analysis in integrated circuits. Dr. Kovács-Vajna is author or coauthor of two books, of more than 50 scientific papers in edited books, international journals and conference proceedings, and of five patents. He is a senior member of the IEEE.